(Received 29 January 2024, Accepted 26 March 2024, Scheduled 7 April 2024)

Active Magnetic Bearing Three-Level Modulation Strategy Based on Mixed Logical Dynamical Model Prediction Controller

Yu Zou[1], Yongqiang Jiang[2], Fan Yang[2,*], Ye Yuan[2], and Fuguang Wen[1]

[1]*Nanjing SAC Power Grid Automation Co., Ltd., Nanjing 211153, China*
[2]*School of Electrical and Information Engineering, Jiangsu University, Zhenjiang 212013, Jiangsu, China*

ABSTRACT: Active magnetic bearings feature advantages of frictionlessness, low loss, and high reliability, making them extensively utilized in fields such as flywheel energy storage, aerospace, and beyond. However, conventional modulation strategies applied to digital control systems suffer from control delays, reducing current control precision and resulting in increased current ripple. To address the aforementioned issues, firstly, the operating principle of the active magnetic bearing drive system is analyzed. Based on hybrid systems theory, a mix logical dynamic model of the drive system is established by introducing auxiliary logical variables and auxiliary continuous variables to achieve three-level modulation. Secondly, integrating model predictive control theory, the established model is utilized as a predictive model to forecast and compensate for control delays in controlling current. Finally, a cost function is established based on the error between predicted current and reference current, and optimal control signals are generated to achieve precise control of the active magnetic bearings. The simulation results demonstrate that under light load conditions, the modulation strategy proposed in this paper reduces current ripple by 49.94% compared to traditional modulation strategies. Under moderate load conditions, the proposed modulation strategy reduces current ripple by 49.96%, while under heavy load conditions, it reduces current ripple by 49.99%. This validates the effectiveness of the proposed modulation strategy in compensating for control delays while retaining the three-level modulation scheme.

1. INTRODUCTION

Magnetic bearings (MBs) [1–7] are high-performance bearings that utilize electromagnetic forces to suspend rotating shafts in space. In contrast with traditional bearings, they offer numerous advantages, including frictionless operation, no need for lubrication, minimal losses, high rotational speeds, and active controllability. Consequently, they find widespread applications across various industrial domains, such as flywheel energy storage and aerospace.

The drive circuit for Active MBs (AMBs) can adopt either a two-level modulation strategy or a three-level modulation strategy. The two-level modulation strategy primarily includes current hysteresis control [8, 9], pulse width modulation (PWM) control [10, 11], and sample-hold control [12]. In particular, current hysteresis control involves feeding the error between feedback and reference currents into a hysteresis comparator to generate PWM signals, thereby controlling the switching of the transistors. PWM control uses a proportional integral (PI) controller to generate an error signal from the feedback and reference current errors, intersecting with the triangular wave from the PWM generator module to produce the control signal for the transistors. Sample-hold control compares the error between the fixed sampling periods of the reference and feedback currents, determining the transistor switching on the basis of the positivity or negativity of their difference. However, employing a two-level modulation strategy in the drive circuit of MBs results in difficulties reducing current ripples [13].

Zhang et al. from the Swiss Federal Institute of Technology in Zurich spearheaded the research on the application of a three-level modulation strategy in drive circuits for MBs. Unlike in two-level modulation, the MB drive circuit under three-level modulation exhibits three states: charging, discharging, and freewheeling. Its control current ripple is decoupled from the bus voltage and is directly proportional only to the conduction voltage drop of the switches and the coil voltage drop [14]. Wang et al. from Tsinghua University proposed a space vector control technology based on three-level modulation to reduce the current ripple and the number of bridge arms [15]. Tang et al. from Nanjing University of Technology proposed a three-level sampling/hold modulation technique, which, building upon the foundation of two-level sampling/hold modulation, introduces a new controllable point within one cycle, thereby achieving three-level modulation in the drive circuit and significantly reducing current ripple [16]. Zhang and Fang from Beihang University conducted a detailed analysis of the mechanism behind current ripple generation and introduced a three-level PWM modulation method for AMBs. This modulation method utilizes a PI controller and a PWM generator to realize duty cycles, separately controlling power switches on diagonals, resulting in a substantial reduction in current ripple [17]. However, traditional three-level modulation strategies for AMBs encounter control latency issues that impact the effectiveness of current ripple suppression [18, 19]. Li et al. from Air Force Engineering University points out that the traditional switching function model only describes the control transition of the circuit and ignores the conditional transition of the circuit,

* Corresponding author: Fan Yang (1000006774@ujs.edu.cn).

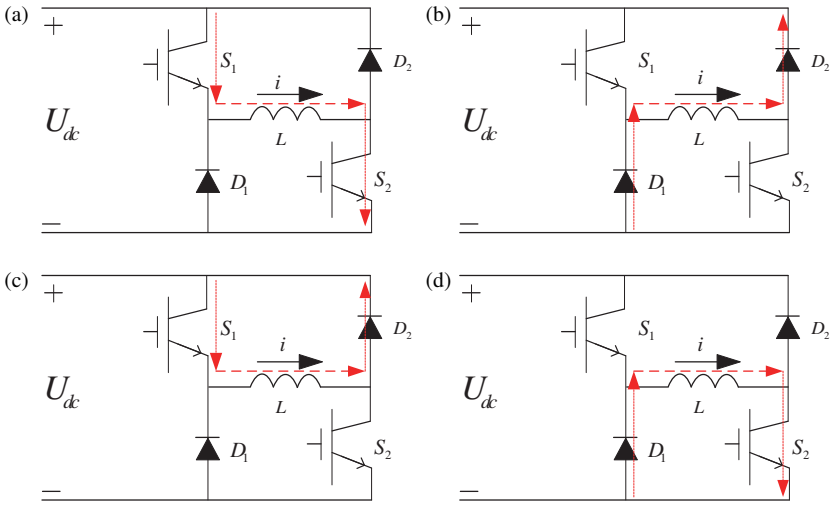

FIGURE 1. Four modes of operation.

while the mix logic dynamic (MLD) model of the three-phase inverter circuit can be effectively described, and combined with the model predictive control strategy, the voltage output harmonics of the three-phase inverter circuit can be effectively reduced [20]. Marandi et al. from Tarbiat Modares University analyzes the hybrid characteristics of the power grid and establishes a mix logic dynamic model of the microgrid, which effectively reduces voltage fluctuation and energy loss as well as battery charging and discharging times with the cost function of minimum charging times and energy loss [21].

This study proposes a three-level modulation strategy for AMBs based on a mixed logical dynamic model prediction controller (MLD-MPC) addressing the aforementioned issues. First, leveraging hybrid system theory [22–26], this study establishes a mixed logical dynamic model of the drive system. This model unifies the mathematical relationship between switch states and control currents during charging, discharging, and freewheeling modes within the driving circuit by introducing auxiliary logical and continuous variables. Second, within the AMB's dual closed-loop control framework, a hybrid logical dynamic predictive controller targeting the inner loop current is designed. This controller calculates predictive control currents to compensate for control latency, incorporating them into the cost function to derive optimal control signals. Lastly, an AMB control system is constructed to validate the proposed strategy's ability to effectively reduce the impact of control latency on current ripple suppression while preserving the three-level modulation mechanism.

2. PRINCIPLE OF THREE-LEVEL MODULATION IN AMB DRIVE CIRCUITS

The drive circuit for AMBs can be implemented in either a half-bridge or full-bridge (H-bridge) configuration. This study focuses on AMB. In consideration of the requirement of bidirectional current capability in the winding, a half-bridge configuration is chosen. Under the three-level modulation strategy, the half-bridge drive circuit presents four distinct operational modes, as illustrated in Figure 1.

In Figure 1(a), the circuit represents the charging state of the drive circuit, where U_{dc} is applied across both ends of the winding, resulting in a linear increase in the winding current. The circuit equation can be expressed as follows:

$$L\frac{di(t)}{dt} + Ri(t) + 2U_{\mathrm{on}} = U_{\mathrm{dc}}, \tag{1}$$

where U_{dc} is the DC bus voltage, U_{on} the switching tube on-voltage drop, L the winding inductance, and r the winding resistance.

The resulting winding current under this charging state can be derived as follows:

$$i(t) = \frac{U_{\mathrm{dc}} - 2U_{\mathrm{on}}}{R}\left(1 - e^{-\frac{t}{\tau}}\right) + i_{\mathrm{a0}}e^{-\frac{t}{\tau}}, \tag{2}$$

where τ is the time constant defined as $\tau = L/R$, and i_{a0} represents the initial winding current at the onset of mode (a).

In Figure 1(b), the circuit represents the discharging state of the drive circuit, where U_{dc} is applied across both ends of the winding, resulting in a linear decrease in the winding current. The circuit equation can be expressed as follows:

$$L\frac{di(t)}{dt} + Ri(t) + 2U_{\mathrm{VD}} = -U_{\mathrm{dc}}. \tag{3}$$

where U_{VD} is the positive pilot voltage drop of the continuous current diode.

The expression for the winding current in the discharging state can be derived as follows:

$$i(t) = -\frac{U_{\mathrm{dc}} + 2U_{\mathrm{VD}}}{R}\left(1 - e^{-\frac{t}{\tau}}\right) + i_{\mathrm{b0}}e^{-\frac{t}{\tau}}, \tag{4}$$

where i_{b0} represents the initial winding current at the onset of mode (b).

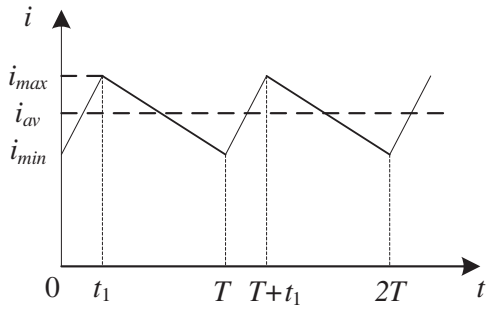

FIGURE 2. Trend of output current of three-level modulation drive circuit.

In Figures 1(c) or 1(d), the drive circuit represents the freewheeling state where the voltage across both ends of the winding is 0. Owing to the presence of winding resistance, the winding current decreases gradually. The current equation can be expressed as follows:

$$L\frac{di(t)}{dt} + Ri(t) + U_{\text{on}} + U_{\text{VD}} = 0. \tag{5}$$

The expression for the current in this freewheeling state can be derived as follows:

$$i(t) = -\frac{U_{\text{on}} + U_{\text{VD}}}{R}\left(1 - e^{-\frac{t}{\tau}}\right) + i_{\text{c0}}(i_{\text{d0}})e^{-\frac{t}{\tau}}, \tag{6}$$

where i_{c0} (i_{d0}) represents the initial winding current at the onset of mode (c) [mode (d)]

During stable operation, the AMB drive circuit under three-level modulation experiences conduction and freewheeling states, with the current trend illustrated in Figure 2. One complete research cycle involves a conduction state, lasting from time 0 to t_1, and a freewheeling state, persisting from t_1 to T.

When the drive circuit is in the charging state, the current reaches its maximum value (i_{max}) at time t_1, i.e.,

$$i_{\text{max}} = \frac{U_{\text{dc}} - 2U_{\text{on}}}{R} + \left(i_{\text{min}} - \frac{U_{\text{dc}} - 2U_{\text{on}}}{R}\right)e^{-\frac{t_1}{\tau}} \tag{7}$$

When the drive circuit is in the freewheeling state, the winding current reaches its minimum value (i_{min}) at time T, i.e.,

$$i_{\text{min}} = -\frac{U_{\text{on}} + U_{\text{VD}}}{R} + \left(i_{\text{max}} + \frac{2U_{\text{on}}}{R}\right)e^{-\frac{T-t_1}{\tau}}. \tag{8}$$

Combining Equations (7) and (8), the expression for the current ripple (Δi) in MBs under the three-level modulation strategy can be obtained as

$$\Delta i = i_{\text{max}} - i_{\text{min}} = \frac{(U_{\text{on}} + Ri + U_{\text{VD}})(U - 2U_{\text{on}} - Ri)}{2L(U - U_{on} + U_{\text{VD}})}T. \tag{9}$$

The conduction voltage drop across the switches and the coil voltage drop can be approximated to be negligible compared with the direct current bus voltage. Hence, under the three-level modulation strategy, the AMB's control current ripple (Δi) can be approximated as

$$\Delta i = i_{\text{max}} - i_{\text{min}} = \frac{U_{\text{on}} + Ri + U_{\text{VD}}}{2L}T. \tag{10}$$

The representation of the AMB's control current ripple (Δi) under the two-level modulation strategy [9] is considered, as shown as follows:

$$\Delta i = i_{\text{max}} - i_{\text{min}} = \frac{U_{\text{dc}}}{2L}T. \tag{11}$$

The comparison of Equations (10) and (11) indicates that under three-level modulation, the current ripple is independent of the direct current bus voltage, and its numerical value is significantly smaller than the current ripple observed under the two-level modulation strategy.

However, the analysis conducted above is based on ideal conditions. In actual control processes, a control delay time (Δt) exists, resulting in the control current ripple (Δi) under the three-level modulation strategy becoming:

$$\Delta i = i_{\text{max}} - i_{\text{min}} = \frac{U_{\text{on}} + Ri + U_{\text{VD}}}{2L}(T + \Delta t). \tag{12}$$

From Equation (12), the control delay will cause an increase in the control current ripple.

3. AMB THREE-LEVEL MODULATION STRATEGY BASED ON MLD-MPC

3.1. Basic Principles of the Proposed Modulation Strategy

To mitigate the impact of control delay (Δt) on the effectiveness of suppressing control current ripples, this study proposes an AMB three-level modulation strategy based on MLD-MPC, as illustrated in Figure 3.

The modulation strategy employs a dual-loop control system, comprising a displacement outer loop and a current inner loop. The displacement outer loop processes the error signal between the reference and feedback displacements, transmitting it through a proportion integration differentiation (PID) controller to produce the current inner loop setpoint. MLD-MPC is designed for the current inner loop. This controller takes the collected control current and calculates predictive currents within

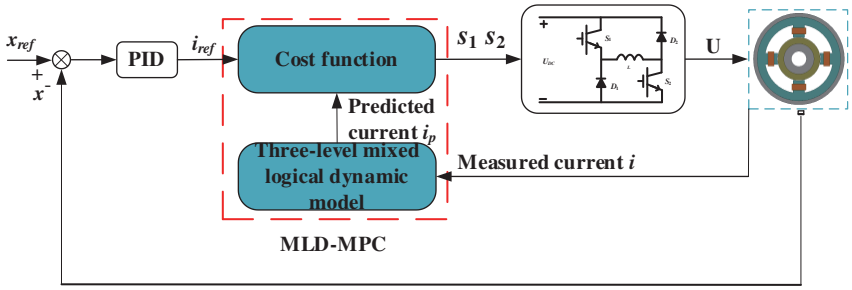

FIGURE 3. Active magnetic bearing three-level modulation strategy based on MLD-MPC.

a predictive model to counteract the effects of control delay. Its objective is to minimize the error between the reference and predicted currents, generating the optimal control signal for the drive circuit. The predictive model integrates a hybrid logical dynamic model of the drive circuit. By incorporating auxiliary logical and continuous variables, this model uniformly represents the mathematical relationship between switch states and control currents in the charging, discharging, and freewheeling modes, facilitating three-level modulation.

3.2. Specific Implementation of the Modulation Strategy

3.2.1. Construction of the MLD Model

The following logical operator symbols are introduced: "v" denotes disjunction; "-" represents negation; and "↔" indicates equivalence. The direction of the current from left to right is defined as positive, and an auxiliary logic variable δ_1 is introduced. $\delta_1 = 1$ signifies the control current $i > 0$, and $\delta_1 = 0$ signifies the control current $i < 0$.

$$\begin{cases} [\delta_1 = 1] \longleftrightarrow [i > 0] \\ [\delta_1 = 0] \longleftrightarrow [i < 0] \end{cases}. \tag{13}$$

When the control current i is greater than 0, the logical relationship between the voltage U across the MB winding and the switch states s_1, s_2, s_3, and s_4 is as follows:

$$\begin{cases} [\delta_1 = 1]\,\mathrm{v}\,[\mathrm{s}_1 = 1]\,\mathrm{v}\,[\mathrm{s}_2 = 1] \longleftrightarrow [\mathrm{U} = \mathrm{U_{dc}}] \\ [\delta_1 = 1]\,\mathrm{v}\,[\mathrm{s}_1 = 1]\,\mathrm{v}\,[\mathrm{s}_2 = 0] \longleftrightarrow [\mathrm{U} = 0] \\ [\delta_1 = 1]\,\mathrm{v}\,[\mathrm{s}_1 = 0]\,\mathrm{v}\,[\mathrm{s}_2 = 1] \longleftrightarrow [\mathrm{U} = 0] \\ [\delta_1 = 1]\,\mathrm{v}\,[\mathrm{s}_1 = 0]\,\mathrm{v}\,[\mathrm{s}_2 = 0] \longleftrightarrow [\mathrm{U} = -\mathrm{U_{dc}}] \end{cases}. \tag{14}$$

The mathematical description of the voltage U across the AMB winding when the control current i is greater than 0 can be derived from Equation (14) as

$$U = \delta_1(s_1 - \overline{s_2})U_{dc}. \tag{15}$$

However, active magnetic bearings do not have current less than 0.

Given auxiliary logic variables δ_2 and δ_3,

$$\begin{cases} \delta_2 = \delta_1 s_1 \\ \delta_3 = \delta_1 \overline{s_2} \end{cases}. \tag{16}$$

The voltage across the MB winding is obtained as

$$U = (\delta_2 - \delta_3)U_{dc}. \tag{17}$$

With auxiliary continuous variables z_1 and z_2,

$$\begin{cases} z_1 = \delta_2 U_{dc} \\ z_2 = \delta_3 U_{dc} \end{cases}. \tag{18}$$

According to the H-bridge circuit equations, the continuous model of the circuit is constructed, and the state equation with the AMB current is established as the state variable, i.e.,

$$\dot{i} = -\frac{R}{L}i + \frac{1}{L}U, \tag{19}$$

where $\dot{i}$ is the derivative of the control current i, R the winding resistance, and U the voltage across the MB winding.

Combining Equations (17), (18), and (19), the original state equation can be transformed into

$$\dot{i} = -\frac{R}{L}i + \frac{1}{L}(z_1 - z_2). \tag{20}$$

The aforementioned state equation involves auxiliary continuous and logic variables. Discretizing Equation (22) yields the MLD model for the AMB drive circuit, as shown as follows:

$$\begin{cases} i_p(k+1) = -\dfrac{RT}{L}i(k) + \dfrac{T}{L}(z_1(k) - z_2(k)) \\ y(k) = i(k) \end{cases}. \tag{21}$$

3.2.2. Selection of Cost Function

MLD-MPC faces the challenge of solving mixed-integer quadratic programming (MIQP) problems. For AMBs, achieving rapid dynamic responses to reach a stable state post-disturbance is crucial. However, solving MIQP problems within extremely short timeframes poses significant difficulties. Given that the H-bridge circuit only presents four distinct operational modes, each corresponding to four different switch state combinations, optimizing control signals involves evaluating these four combinations separately. Comparing their respective cost function values allows the selection of a combination resulting in the minimum cost function value,

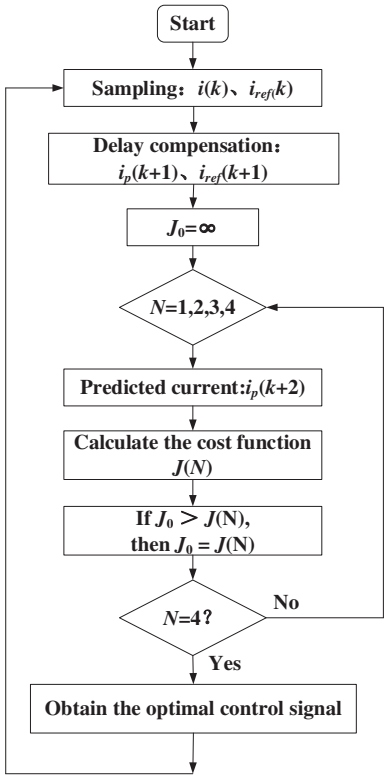

FIGURE 4. Flow chart of control strategy.

thereby minimizing the error in the desired reference current for the AMBs. The established cost function facilitates the selection of the control signal for the MB drive circuit by determining the optimal switch control signal.

$$J = (i_{ref}(k+1) - i_p(k+1))^2, \tag{22}$$

where $i_p(k+1)$ represents the predicted current of the AMB winding at time $k+1$, and $i_{ref}(k+1)$ stands for the given current of the AMB winding at time $k+1$. Although the reference value at time $k+1$ can be approximated to be nearly equal to the reference value at time k, this approximation introduces a delay of one sampling period in the given signal. For enhancing control precision, a second-order Lagrange interpolation method can be utilized to obtain the control current reference value at time $k+1$, as follows:

$$i_{ref}(k+1) = 3i_{ref}(k) - 3i_{ref}(k-1) + i_{ref}(k-2). \tag{23}$$

3.2.3. Control Delay Compensation

Due to the delay in the digital control system [27–29], the selected control signal needs to be output in the next time step. However, at this time, the control current has already become $i_p(k+1)$. Therefore, to eliminate the impact of this delay, it is necessary to predict the current forward one more time with $i_p(k+1)$ as the initial condition and obtain the current prediction value $i_p(k+2)$ at time $k+2$, as follows:

$$i_p(k+2) = -\frac{RT}{L} i_p(k+1) + \frac{T}{L}(z_1(k+1) - z_2(k+1)). \tag{24}$$

Thus, the cost function can be redefined as:

$$J = (i_{ref}(k+2) - i_p(k+2))^2, \tag{25}$$

where $ip(k+2)$ is the predicted current of the MB winding at time $k+2$, and $i_{ref}(k+2)$ is the predicted reference current of the MB winding at time $k+2$, which can be obtained by forward derivation from Equation (25).

$$i_{ref}(k+2) = 3i_{ref}(k+1) - 3i_{ref}(k) + i_{ref}(k-1). \tag{26}$$

3.2.4. Flowchart of the Control Strategy

Figure 4 shows the flowchart of the predictive control strategy, consisting of the following steps:

1. Sample the current moment's current $i(k)$ and reference current $i_{ref}(k)$.
2. Compensate for the delay in the AMB control system by predicting the values of current $i_p(k+1)$ and $i_{ref}(k+1)$ at time $k+1$.
3. For the four different switch state combinations, predict the control current using the forecasting model in Equation (26), and then calculate the value of the cost function in Equation (25).
4. The four cost functions are compared, and the minimum cost function is selected.
5. Select the switch state combination corresponding to the minimum cost function value, which represents the opti-

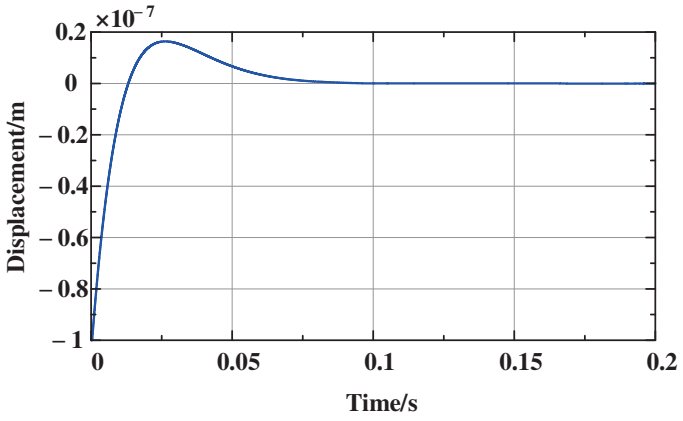

FIGURE 5. Displacement waveform during floating.

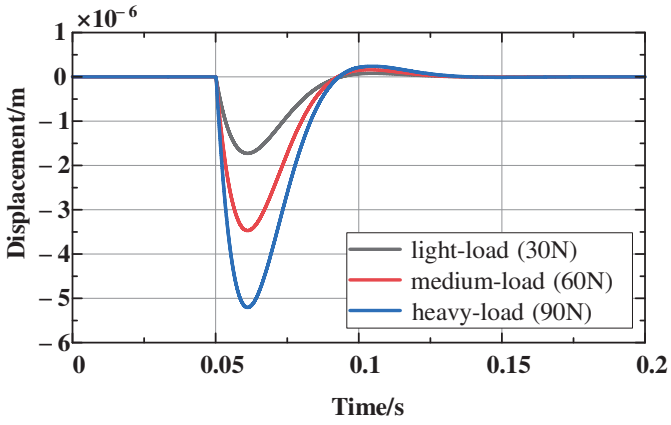

FIGURE 6. Displacement waveforms under different loads.

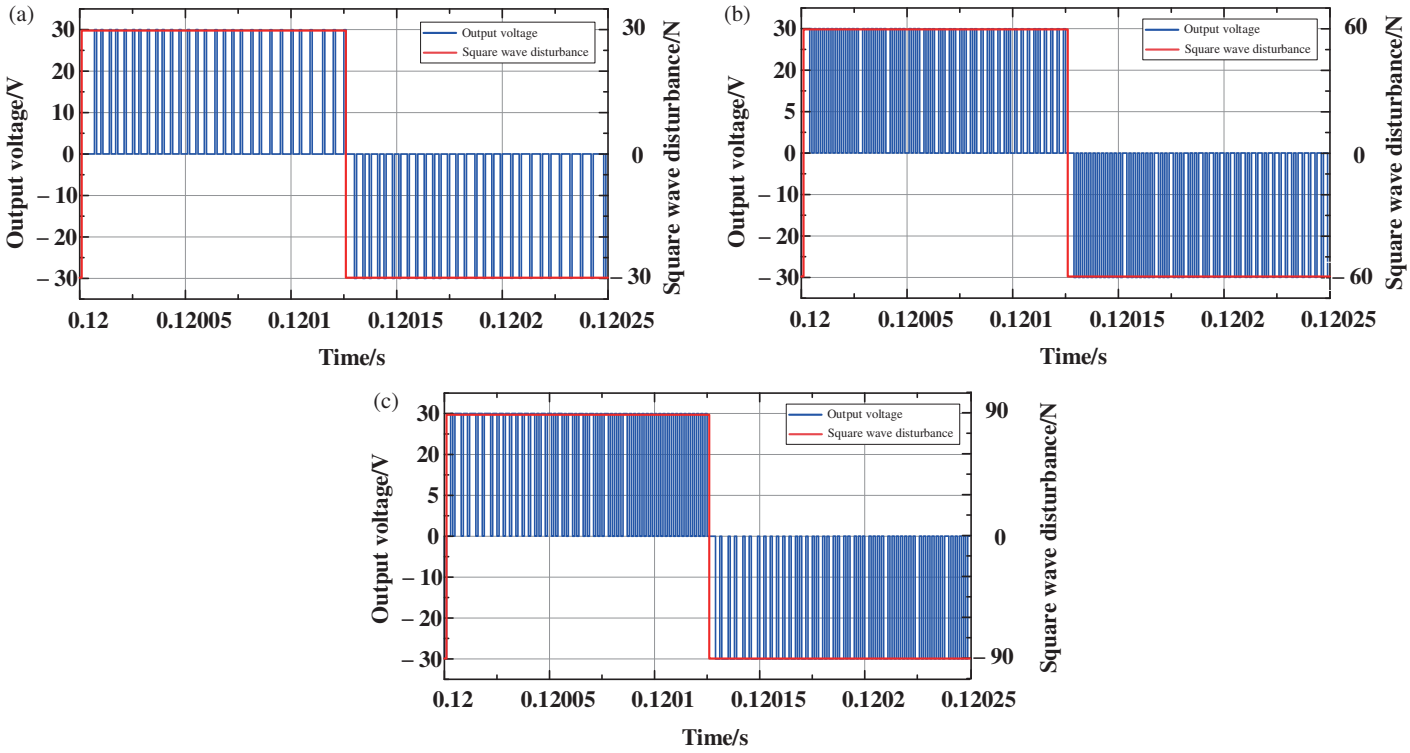

FIGURE 7. Voltage output waveform under different square wave disturbances. (a) (a) Square wave disturbances of ±30 N. (b) Square wave disturbances of ±60 N. (c) Square wave disturbances of ±90 N.

mal control signal for the drive circuit, and proceed to the next iteration in the algorithm.

4. STRATEGY VALIDATION

Using MATLAB/Simulink for simulation validation of the proposed method, this study determines the simulation parameters as follows: $U_{dc} = 30$ V, inductance in the coil $L = 2.8$ mH, coil resistance $r = 1.3\,\Omega$, sampling period $T = 1$ µs, and maximum load of 100 N.

4.1. Validation of Control System Effectiveness

The control system is validated via a levitation test. Figure 5 illustrates the displacement waveform during rotor levitation in the AMB control system.

During the process from the initiation of AMB suspension to a stable operation, the maximum displacement reaches 2.0×10^{-8} m. After 0.09 s, the displacement returns to the equilibrium position. During the stable operation, a fluctuation with an amplitude of 3.0×10^{-11} m is observed, indicating a high level of levitation precision.

As depicted in Figure 6, upon introducing a light-load (30 N) disturbance at 0.05 s, the system under the modulation strategy

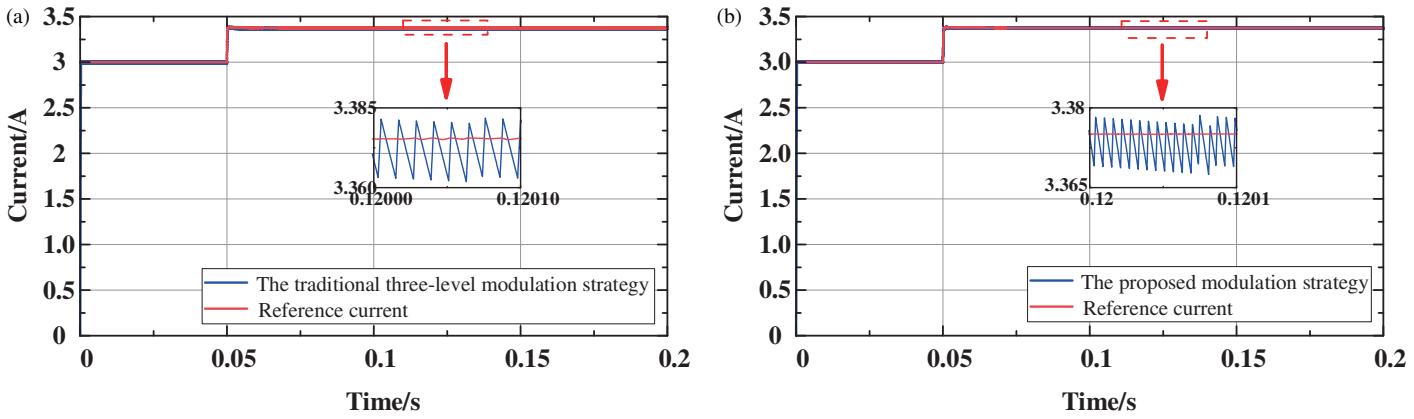

FIGURE 8. Comparison of Current waveform at light-load (30 N). (a) The traditional three-level modulation strategy. (b) The proposed modulation strategy.

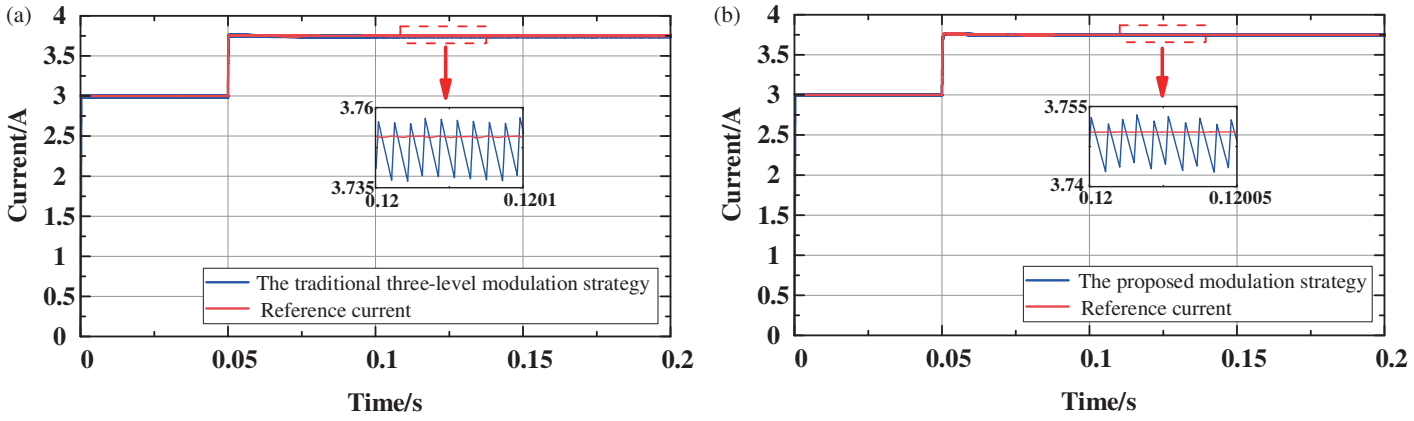

FIGURE 9. Comparison of Current waveform at medium-load (60 N). (a) The traditional three-level modulation strategy. (b) The proposed modulation strategy.

proposed in this paper experiences a displacement fluctuation of -1.74×10^{-6} m. It returns to the equilibrium position after 0.08 s. At 0.05 s, with the introduction of a medium-load (60 N) disturbance, the system under the proposed modulation strategy experiences a displacement of -345×10^{-6} m. It returns to the equilibrium position after disturbance, and the system under the proposed modulation strategy exhibits a displacement of -5.2×10^{-6} m. It reverts to the equilibrium position after 0.1 s.

The control system based on the proposed modulation strategy demonstrates robustness when being subjected to light-load, medium-load, and heavy-load.

4.2. Feasibility Validation of Three-Level Modulation

The feasibility validation of the control system's three-level modulation is conducted. Square wave disturbances of ± 30, ± 60, and ± 90 N are applied to the control system, and the voltage output of the drive circuit is depicted in Figure 7.

From Figure 7(a), under the ± 30 N square wave disturbance, the drive circuit outputs positive and zero voltages in the positive half-cycle and negative and zero voltages in the negative half-cycle. Similarly, under the ± 60 and ± 90 N square wave disturbances, the drive circuit outputs positive and zero voltages in the positive half-cycle and negative and zero voltages in the negative half-cycle.

In conclusion, under different square wave disturbances, the drive circuit consistently outputs positive, negative, and zero voltages within one cycle, verifying that the control system can achieve three-level modulation.

4.3. Effective Validation of Control Delay Suppression

The effectiveness of the proposed modulation strategy in suppressing control delays is validated. Faced with light-load (30 N), medium-load (60 N), and heavy-load (90 N), the current waveforms under the traditional AMB three-level modulation strategy [30] and the proposed strategy are depicted in Figures 8 to 10, respectively.

From Figure 8, when facing a light-load (30 N) disturbance, the control current ripple of the AMB under the traditional three-level modulation strategy is 1.827×10^{-2} A. Under the proposed modulation strategy, the current ripple decreases to 9.145×10^{-3} A, marking a 49.94% decrease.

Figure 9 demonstrates that when encountering a medium-load (60 N) disturbance, the control current ripple of the MB

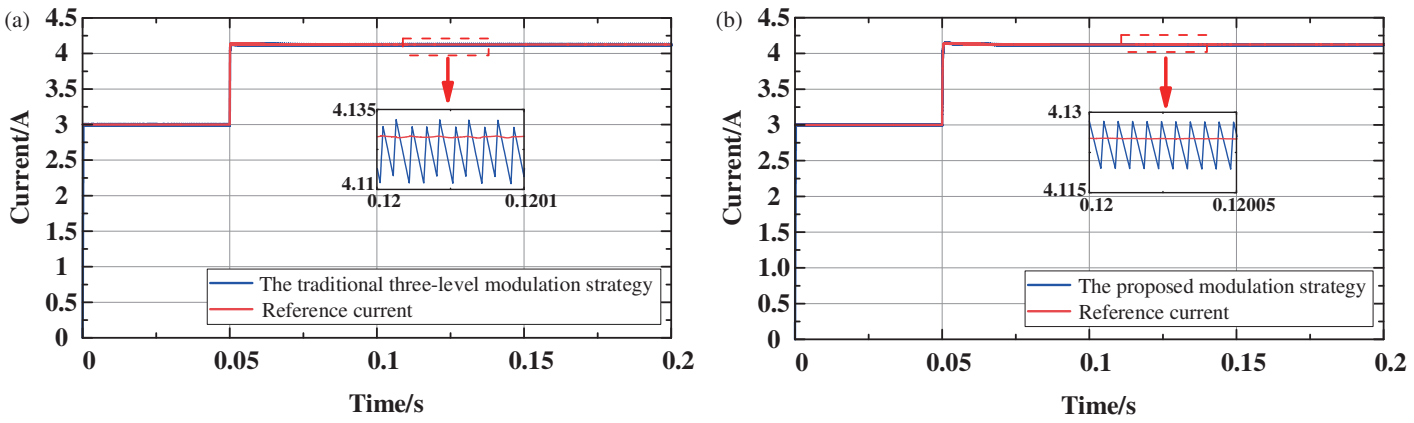

FIGURE 10. Comparison of Current waveform at heavy-load (90 N). (a) The traditional three-level modulation strategy. (b) The proposed modulation strategy.

under the traditional three-level modulation strategy is 1.793×10^{-2} A. By contrast, the proposed modulation strategy yields a current ripple of 8.972×10^{-3} A, marking a reduction of 49.96%.

From Figure 10, when being faced with a heavy-load (90 N) disturbance, the control current ripple of the AMB under the traditional three-level modulation strategy measures 1.759×10^{-2} A. On the contrary, the proposed modulation strategy yields a current ripple of 8.796×10^{-3} A, marking a reduction of 49.99%.

In summary, compared with the above two traditional three-level modulation strategies, the three-level modulation strategy based on MLD-MPC can effectively compensate a sampling period control delay and further reduce the control current ripple under light-load, medium-load, or heavy-load disturbance.

5. CONCLUSION

An MB three-level modulation strategy based on MLD-MPC is proposed, yielding the following conclusions:

1. Based on the theory of hybrid systems, a mixed logical dynamic model can be established to characterize the charging, discharging, and freewheeling states of the AMB drive circuit uniformly.

2. The AMB three-level modulation strategy based on MLD-MPC effectively suppresses control delay and reduces current ripple.

ACKNOWLEDGEMENT

This work was sponsored in part by National Natural Science Foundation of China (52377053), Key research and development program of Jiangsu Province (BE2021094), China Postdoctoral Science Foundation (2021M702413) & Priority Academic Program Development of Jiangsu Higher Education Institutions (No. PAPD-2018-87).

REFERENCES

[1] Xiang, B., X. Wang, and W. O. Wong, "Process control of charging and discharging of magnetically suspended flywheel energy storage system," *Journal of Energy Storage*, Vol. 47, 103629, 2022.

[2] Yang, I.-J., M.-K. Hong, J. Lee, W.-H. Kim, and D.-H. Jung, "Design for reducing bearing force ripple and torque ripple of integrated magnetic bearing motor through halbach array," *Energies*, Vol. 16, No. 3, 1249, 2023.

[3] Ma, Z. and H. Q. Zhu, "Research and development overview of key technologies on inverter driven magnetic bearings," *Proceedings of the CSEE*, Vol. 43, No. 19, 7649–7659, 2023.

[4] Liu, C., J. Zhan, J. Wang, Y. Yang, and Z. Liu, "An improved one-cycle control algorithm for a five-phase six-leg switching power amplifier in active magnetic bearings," *IEEE Transactions on Industrial Electronics*, Vol. 69, No. 12, 12 564–12 574, Dec. 2022.

[5] Liu, G., J. Huan, H. Zhu, C. Zhao, and Z. Ma, "Decoupling control of six-pole hybrid magnetic bearings," *Progress In Electromagnetics Research M*, Vol. 109, 51–61, 2022.

[6] Zhang, W. Y., H. Q. Zhu, and Y. Yuan, "Study on key technologies and applications of magnetic bearings," *Transaction of China Electrotechnical Society*, Vol. 30, No. 12, 12–20, 2015.

[7] Jiang, H., Z. Su, and D. Wang, "Analytical calculation of active magnetic bearing based on distributed magnetic circuit method," *IEEE Transactions on Energy Conversion*, Vol. 36, No. 3, 1841–1851, 2020.

[8] Xu, Z., D.-H. Lee, and J.-W. Ahn, "Control characteristics of 8/10 and 12/14 bearingless switched reluctance motor," in *2014 International Power Electronics Conference (IPEC-Hiroshima 2014 - ECCE ASIA)*, 994–999, Hiroshima, Japan, 2014.

[9] Yang, F., Y. Yuan, Y. Sun, S. Ding, L. Yan, and J. Xu, "Coupling suspension force regulator considering time-varying characteristic for a bearingless switched reluctance motor," *IEEE Transactions on Industrial Electronics*, Vol. 70, No. 7, 6632–6641, Jul. 2023.

[10] Cao, G. and C. Lee, "Development of PWM power amplifier for active magnetic bearings," in *Fifth World Congress on Intelligent Control and Automation*, 3475–3478, Hangzhou, China, 2004.

[11] Yang, J., D. Jiang, H. Sun, J. Ding, A. Li, and Z. Liu, "A series-winding topology converter with capability of fault-tolerant operation for active magnetic bearing drive," *IEEE Transactions on Industrial Electronics*, Vol. 69, No. 7, 6678–6687, Jul. 2022.

[12] Wu, H. C., X. Zhang, K. Yang, M. Yu, and N. Wang, "Review of magnetic bearing power amplifier," *Research Review on Power Amplifiers for Magnetic Bearings*, Vol. 12, 8–16, 2022.

[13] Yu, Z. L. and C. S. Zhu, "Analysis on the stability of two-level current mode switching power amplifiers," *Transactions of China Electrotechnical Society*, Vol. 34, No. 2, 306–315, 2019.

[14] Zhang, J., J. O. Schulze, and N. Barletta, "Synchronous three-level PWM power amplifier for active magnetic bearings," in *5th International Symposium on Magnetic Bearings*, 277–282, 1996.

[15] Wang, C., Y. Xu, and K. Zhang, "Duty cycle restriction strategies of SVPWM algorithm formagnetic bearing power amplifiers," *Chinese Journal of Scientific Instrument*, Vol. 42, No. 01, 248–256, 2021.

[16] Tang, S. C., G. M. Zhang, and L. Mei, "The research of thethree-level switching power amplifier about the magnetic bearings system," *Power Electronic Technology*, Vol. 49, No. 1, 36–39, 2015.

[17] Zhang, L. and J. Fang, "Analysis of current ripple and implementation of pulse width modulation switching power amplifiers for active magnetic bearing," *Transactions of China Electrotechnical Society*, Vol. 22, No. 3, 13–20, 2007.

[18] Wu, X., W. Song, S. LE, *et al.*, "Model predictive direct current control of induction machines fed by a three level inverter," *Transactions of China Electrotechnical Society*, Vol. 32, No. 18, 113–123, 2017.

[19] Li, C., B. T. Vankayalapati, B. Akin, and Z. Yu, "Analysis and compensation of sigma-delta ADC latency for high performance motor control and diagnosis," *IEEE Transactions on Industry Applications*, Vol. 59, No. 1, 873–885, 2023.

[20] Li, N., Y. Li, J. Han, and X. H. Zhu, "FCS-MPC strategy for inverters based on MLD model," *Power System Technology*, Vol. 38, No. 2, 375–380, 2014.

[21] Marandi, A., A. Ramezani, and R. M. Taleghani, "Hybrid model predictive control strategy of renewable resources in DC microgrids based on mixed logic dynamics and measurements," in *2021 7th International Conference on Control, Instrumentation and Automation (ICCIA)*, 1–5, IEEE, 2021.

[22] Huang, W., J. Du, W. Hua, K. Bi, and Q. Fan, "A hybrid model-based diagnosis approach for open-switch faults in PMSM drives," *IEEE Transactions on Power Electronics*, Vol. 37, No. 4, 3728–3732, Apr. 2022.

[23] Bemporad, A. and M. Morari, "Control of systems integrating logic, dynamics, and constraints," *Automatica*, Vol. 35, No. 3, 407–427, 1999.

[24] Zamani, M. R., Z. Rahmani, and B. Rezaie, "A novel model predictive control for a piecewise affine class of hybrid system with repetitive disturbance," *ISA Transactions*, Vol. 108, 18–34, 2021.

[25] Sun, X., Y. Cai, C. Yuan, S. Wang, and L. Chen, "Vehicle height and leveling control of electronically controlled air suspension using mixed logical dynamical approach," *Science China Technological Sciences*, Vol. 59, 1814–1824, 2016.

[26] Li, X. G. and D. J. Gao, "Moving horizon state feedback predictive control for hybrid system based on mixed logic dynamic," *Acta Automatica Sinica*, Vol. 30, No. 4, 567–571, 2004.

[27] Fan, P. Z., L. Liu, D. S. Jin, and S. Y. Liu, "Optimization algorithm of deadbeat current predictive control for permanent magnet synchronous motor," *Journal of Xi'an Jiaotong University*, Vol. 57, No. 4, 29–38, 2023.

[28] Wu, Z. T. and Z. N. Yang, "Double closed-loop robust compensation control for permanent magnet linear synchronous motor," *Electric Machines and Control*, Vol. 26, No. 3, 101, 2022.

[29] Li, C., B. Vankayalapati, and B. Akin, "Latency compensation of SD-ADC for high performance motor control and diagnosis," in *2021 IEEE 13th International Symposium on Diagnostics for Electrical Machines, Power Electronics and Drives (SDEMPED)*, Vol. 1, 289–294, Dallas, TX, USA, 2021.

[30] Zang, X., X. Wang, and Z. Qiu, "Research on current mode tri-state modulation technology in switching power amplifier for magnetic bearings," *Proceedings of the CSEE*, Vol. 24, No. 9, 167–172, 2004.